https://doi.org/10.1016/j.solmat.2019.02.035

Metal-organic framework derived porous carbon of light trapping structures for efficient solar steam generation

Sainan Ma[1,2], Wayesh Qarony[2], Mohammad Ismail Hossain[2], Cho Tung Yip[3,], Yuen Hong Tsang[1,2,]**

[1] The Hong Kong Polytechnic University Shenzhen Research Institute, Shenzhen, Guangdong, China

[2] Department of Applied Physics, The Hong Kong Polytechnic University, Hung Hom, Kowloon, Hong Kong, China

[3]School of Science, Harbin Institute of Technology, Shenzhen Graduate School, Shenzhen, Guangdong 58055, China

* Corresponding authors.

E-mail: yuen.tsang@polyu.edu.hk (Y. H. Tsang), h0260416@hit.edu.cn (C. T. Yip)

Abstract

Utilizing solar energy to evaporate water is a green and promising approach in addressing the issue of global freshwater shortage and water pollution. Carbon materials have gained extensive research attention as efficient solar absorbers for solar steam generation owing to the non-toxic nature and environmental friendliness. In this work, the metal-organic framework (MOF) derived porous carbon (MDPC) materials were first employed as solar absorbers for

enhancing water evaporation. An efficient surface heating and evaporation system was designed by coating the leaf-like two-dimensional (2D) MOF precursor on stainless steel mesh followed by calcination (MDPC/SS mesh), and then in conjunction with a floating air-laid paper wrapped polyethylene (EPE) foam. The prepared solar evaporator with unique light trapping structures shows a high solar absorption (> 97%), excellent hydrophilicity, and great surface heat localization for solar steam generation. Consequently, a photo-thermal conversion efficiency of 84.3% with an evaporation rate of 1.222 kg m^{-2} h^{-1} was achieved under one sun illumination. Furthermore, the MDPC/SS mesh shows good recyclability and durability. This work opens a new avenue for the application of MOF derived carbon as photo-thermal material in the field of solar steam generation.

Keywords: solar steam generation, metal-organic frameworks, carbon materials, heat localization, light trapping.

1. Introduction

With the fast increasing population and severe environmental issues, fresh water scarcity has become one of the most crucial and essential global challenges [1, 2]. Although 71% of the Earth's surface is covered by water, only 2.5% of that is fresh water [3]. Numerous efforts have been devoted to seeking solutions to address water shortage, among which solar steam generation is expected to be a promising technology for freshwater regeneration as solar energy

is the cleanest and most inexhaustible renewable energy source [4-6]. However, conventional solar steam generation systems usually involve bulk-water heating, relying on the expensive optical concentrators, which are costly for manufacturing and maintenance. Moreover, the energy efficiency of these systems is quite low due to the considerable energy loss [7, 8]. Therefore, it is essential to develop a more efficient solar steam generation system for economic and practical applications.

Recently, interfacial solar steam generation systems using floating evaporators have been widely investigated to generate heat at the air-water interface [9-14]. Previous research shows that plasmonic and carbon-based materials are commonly used as the photo-thermal materials for efficient evaporators [15-19]. For example, a plasmonic film of gold nanoparticles for interfacial solar evaporation with a conversion efficiency of 44% was reported by Deng's group [20]. Besides the gold nanoparticles, Zhu et al. demonstrated a high performance aluminum nanoparticles-based evaporator for efficient solar desalination [21]. However, the metal nanoparticles aggregate and loss functionality easily. Additionally, the noble metals used for plasmon-enhanced evaporators are too expensive for practical use. On the other hand, the carbon-based materials, such as graphene and graphene oxide [22-24], carbon nanotube [25], carbon black [26], wood [27], carbonized mushroom [28], etc. are very promising for solar steam generation due to their high solar light absorptions and eco-friendly characteristics. For instance, Zhou and co-workers reported a flame-treated wood for solar steam generation with

a solar conversion efficiency of 72% [27]. Wang et al. designed a bilayer RGO-based membrane to drive a solar thermal conversion efficiency of 83% [29]. The photo-thermal conversion efficiency among some of these materials has also reached over 80% under one sun illumination. Nevertheless, the graphene or CNT based materials are complicated to fabricate. Wood is a natural material that could also suffer from structural irregularity and natural decay, leading to performance instability. Thus, novel carbon materials with rational structure designs should be further developed, which offer a new degree of freedom in designing solar thermal absorber for efficient solar steam generation.

Recently, metal-organic frameworks (MOFs), a new class of organic-inorganic hybrid crystalline materials, have drawn tremendous interest from the researchers [30, 31]. Thanks to the enormous surface areas, high porosity, and flexible composition, MOFs have been proved to be the valuable templates or precursors for the synthesis of porous carbon [32], metal oxides [33, 34], metal or metal oxides/carbon [35]. Among them, MOF-derived porous carbons (MDPC) have been widely employed across many disciplines, including catalysis [36, 37], gas storage and separation [32], oil/water separation [38], and sensors [39]. As a member of carbon materials, MDPC can be a promising participant for solar steam generation, which is nontoxic and environmentally friendly. Compared to other carbon materials like woods which decompose especially in the wet environment, MDPC is a more reliable and stable carbon material. In addition, the structural diversity of MOF is enormous [31], allowing to utilize them

in various forms of structures, whereas graphene and CNT do not exhibit such diverse forms of structures. Moreover, the porous frameworks in MDPC can be valuable for light harvesting and vapor escaping in solar steam generation, which are missing in most of the reported carbon materials. Nevertheless, to the best of our knowledge, the application of MDPC in solar steam generation has not yet been reported.

In this work, we report a novel solar evaporator composed of MDPC coated SS mesh (MDPC/SS mesh) supported by air-laid paper wrapped polyethylene (EPE) foam for the first time. The MDPC/SS mesh was prepared by a facile solvent reaction process to deposit the leaf-like MOF precursor on SS mesh and then followed by an annealing process to obtain the porous carbon, exhibiting an enhanced light trapping effect. The evaporation mechanism and performance enabled by the EPE foam supported MDPC/SS mesh are characterized and discussed. This free-floating evaporator shows high photo-thermal conversion efficiency and good recyclability and stability for solar steam generation under one sun illumination. The superior performance allows the MDPC/SS mesh for a potential application in solar-driven seawater desalination.

2. Experimental

2.1. Materials

Cobalt nitrate hexahydrate ($Co(NO_3)_2 \cdot 6H_2O$), 2-methylimidazole (2MIM), and acetic acid were purchased from Sigma-Aldrich. Ethanol with ACS grade was bought from the Anaqua

Global International Inc., Ltd. All chemicals were used without further purification. Stainless steel (SS) meshes (400 mesh size, thickness of 250 μm) were obtained from the Anping Metal Mesh Manufactory. The mixed cellulose esters (MCE) membrane (pore size of 0.22 μm) was provided by Shanghai Xinya Co., Ltd. Deionized (DI) water was used throughout all experiments generated from a Millipore system.

2.2. Preparation of MOF/SS mesh

The 2D leaf-like MOF coated SS mesh was prepared referring to the previous literatures [40, 41]. Briefly, 40 ml of pre-prepared 2MIM aqueous solution (0.4 M) was quickly added into a pink solution of $Co(NO_3)_2 \cdot 6H_2O$ (40 mL, 50 mM), then a piece of pre-treated SS mesh (2*2 cm^2, washed by sonicating in ethanol, DI water, and 1.0 M acetic acid for 20 mins, respectively) was immersed into the mixture and kept for 1 h at the room temperature. Then the SS mesh was taken out, washed by ethanol and DI water for several times, and then dried overnight.

2.3. Preparation of MDPC/SS mesh

The pre-prepared 2D MOF coated SS mesh was carbonized through annealing in 100 sccm Ar atmosphere at 700 ℃ for 2 h with a heating rate of 5 ℃ min^{-1}. The MDPC/SS mesh was finally obtained after naturally cooling down to room temperature under the Ar atmosphere.

2.4. Preparation of MDPC film

The MOF powders were obtained through the as-mentioned method without immersing the SS mesh, in which the mixed solution kept for 1 h was centrifuged. The obtained purple powders

were dried overnight and then annealed through the same process. Then the as-prepared black MDPC powders were dispersed in DI water, following by vacuum filtration on the MCE membrane.

2.5. Characterization

SEM images were obtained using a field-emission scanning electron microscope (JEOL, JSM-6490) with an accelerating voltage of 5 kV. TEM images were acquired from the field-emission transmission electron microscope (JEOL, JEM-2100F). The reflection spectra were collected through an UV-vis-NIR spectrophotometer (UV-3600), equipped with an integrating sphere. The Raman spectra were measured through a Raman spectroscopy (Horiba Jobin Yvon, HR800) with an excitation laser source of 488 nm. The surface hydrophilic property of the sample was valued by a contact-angle analyzer (SDC-350). The temperature distribution images were recorded by an IR camera (Fluke, Model Ti400, USA).

2.6. Evaluation of the solar evaporation and solar desalination

All the solar water evaporation experiments were conducted under a 300 W Xenon lamp (PLS-SXE300, Perfect light, Beijing) with an AM 1.5 filter to simulate the solar irradiance. The light intensity at the sample surface is adjustable. The optical power on the surface was measured by a power meter (THORLABS, S314C). For solar evaporation, the solar absorber samples were placed on top of a cylindrical container filled with DI water. To evaluate the water evaporation performances of the solar absorber, the weight loss of the cylindrical container was

monitored over time by using a computer controlled electronic balance (Mettler Toledo, ME201, 0.1 mg). Moreover, a homemade setup was designed to analyze the solar desalination. The evaporated water was condensed and run down on the cold chamber wall. All experiments were performed under a room temperature of 21 ±1℃ and humidity of about 70%.

3. Results and discussion

The fabrication process of the MDPC/SS mesh-based evaporator for solar evaporation is schematically shown in Fig. 1. The 2D MOF was directly coated onto the SS mesh via a simple solution method. Then the silver-white SS mesh turned into purple after the deposition of 2D MOF, and later turned into completely black after annealing, indicating the high light absorption (Fig. S1). SS mesh was chosen as the substrate due to its good mechanical strength, high heat resistance for the annealing process, as well as low cost for its abundance. The MDPC/SS mesh used as the light absorbing layer was then put on the surface of an EPE foam which was tightly wrapped by air-laid paper. To ensure a good contact between the MDPC/SS mesh and the air-laid paper wrapped EPE foam, the surface of the EPE foam should be flat and a gentle pressure should be applied during placing the MDPC/SS mesh onto the EPE foam. In this design, the water can be transported upward spontaneously through the air-laid paper and spread throughout the MDPC/SS mesh, where the EPE foam serves as a thermal insulator.

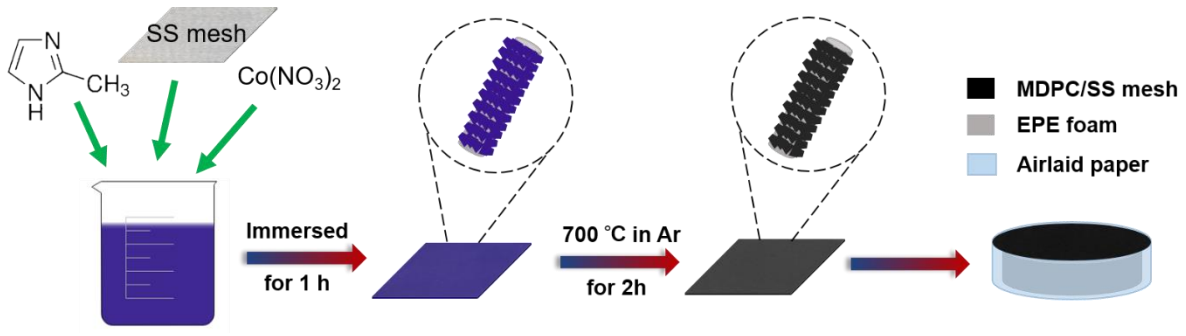

Fig. 1. The fabrication process of the MDPC/SS mesh-based evaporator. The silver SS mesh turned into purple for the deposition of leaf-like MOF precursor, and then turned into black after annealing.

The morphologies of the sample were characterized by SEM. Fig. 2a shows the SEM images of the bare commercial SS mesh, of which the wire surface is smooth. After the deposition of 2D MOF, the wire surface of the SS mesh is entirely covered with leaf-like vertical aligned plate arrays as shown in Fig. 2b. The morphology of the MOF coated SS mesh after annealing is shown in Fig. 2c. The MOF precursor decomposed during the annealing process. Thus the resultant plate arrays became thinner, but the leaf-like vertical aligned structural units were well retained. The TEM image in Fig. 2d clearly shows that the MDPC sheet is composed of porous carbon with many nanoparticles. These unique structures are supposed to increase the surface roughness for light-trapping effect for solar energy absorption. As the evaporation occurs at the air-water surface, solar evaporators with the hydrophilic surface are essential for continuously moving liquid to the heated area [42]. The surface hydrophilicity of the MDPC/SS mesh was valued by dropping a water droplet (5 μL) on the surface of the sample. Fig. 2e

illustrates the water droplet spread out instantly (<50 ms) on the MDPC/SS mesh, demonstrating the high hydrophilic property of the obtained MDPC/SS mesh.

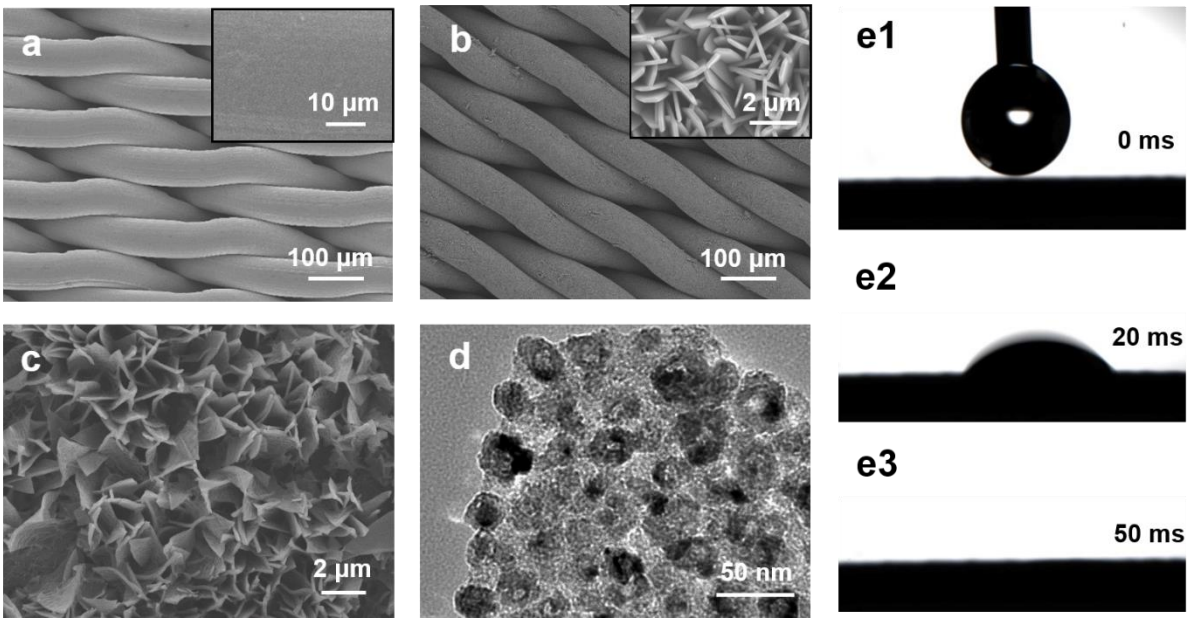

Fig. 2. The SEM images of (a) bare SS mesh, (b) MOF coated SS mesh, and (c) MDPC/SS mesh. (d) TEM image of the MDPC nanosheet scraped from the MDPC/SS mesh. (e) Water contact angles of the MDPC/SS mesh during different shoot time.

To determine the intrinsic optical properties of the MDPC/SS mesh, its reflection and transmission spectra were obtained by a UV-vis-NIR spectrophotometer equipped with an integrating sphere. As shown in Fig. 3a, the MDPC/SS mesh displays an extremely low reflectance of less than 3%, while the transmission is nearly nonexistent in the range of 250 nm to 2500 nm (covering the majority of the solar spectrum) as provided in the supplementary file

(Fig. S2). Because that the SS mesh is made via the craft of twill weave of the metal wires (Fig. 2a), it blocks light transmission while water can still penetrate. The results show that the synthesized MDPC/SS mesh processes excellent broadband light absorption as high as 97% for the incident solar energy spectrum (Fig. 3b). This merit can be attributed to the multi-scattering and light trapping effect due to the vertically aligned nanoplate array architecture and the inside nanoporous frameworks. The flat surface usually leads to a distinctly high reflection of the incident light as illustrated in Fig. 3c. However, the incident light in such nanostructure can bounce back and forth between the vertically aligned carbon arrays and inside the nanopores of the carbon frameworks, resulting in an enhanced optical path length of the incident light. As a consequence of that, the absorption of light in the absorbing layer and the solar energy conversion efficiency can be increased in comparison with the planar surface. In addition, the MDPC/SS mesh was further investigated by Raman spectra and included in the Supplementary Fig. S3. The obtained MDPC/SS mesh displays two characteristic peaks of carbon materials assigned to D-bands of 1350 cm^{-1} and G-bands of 1580 cm^{-1}, which are consisted with the previous works [43, 44].

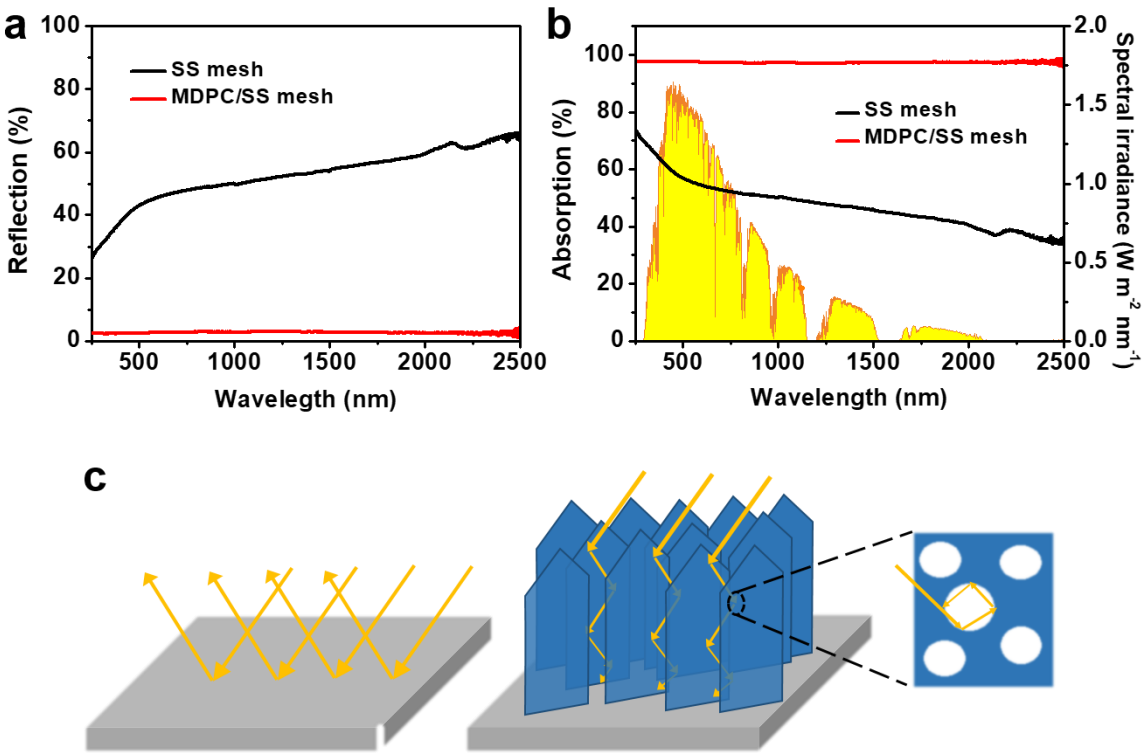

Fig. 3. (a) Reflection and (b) absorption spectra of the bare SS mesh and MDPC/SS mesh. (c) Schematic diagram of light trapping effect due to the nanoplate array architecture and nanoporous frameworks of the MDPC.

The photo-thermal property of the MDPC/SS mesh was further investigated, where the top-view and cross-sectional temperature distribution of the cylindrical container with and without MDPC/SS mesh floating on the surface under the simulated solar light of 1 kW m^{-2} were recorded by an IR camera. The MDPC/SS mesh was supported by an air-laid paper wrapped EPE foam to float on the water surface. As seen in Fig. 4a1 and 4b1, before irradiation, the surface temperatures of pure water and MDPC/SS mesh-foam were closed to that of ambient

temperature. After 30 min of irradiation, the surface temperatures of both systems reached a stable condition. IR images in Fig. 4b2 shows that the surface temperature of the system with MDPC/SS mesh reached at ~37 ℃ (increased by 16 ℃), whereas the temperature of pure water only increased by 5 ℃ (Fig. 4a2). From the cross-sectional IR images in Fig. 4a3, pure water showed an obvious increase in bulk water temperature. While floating the MDPC/SS mesh-foam, there was a clear temperature gradient between the top surface of the MDPC/SS mesh and underlying bulk water as shown in Fig. 4b3. In our structure, the air-laid paper wrapped EPE foam prevents the direct contact of the MDPC/SS mesh with bulk water. Thus, the generated heat can be highly localized at the top surface layer, while the heat loss to the bulk water is suppressed. Such design utilizing low-dimensional water pathways to achieve surface evaporation with high photo-thermal conversion efficiency is promising for efficient solar steam generation [45-48].

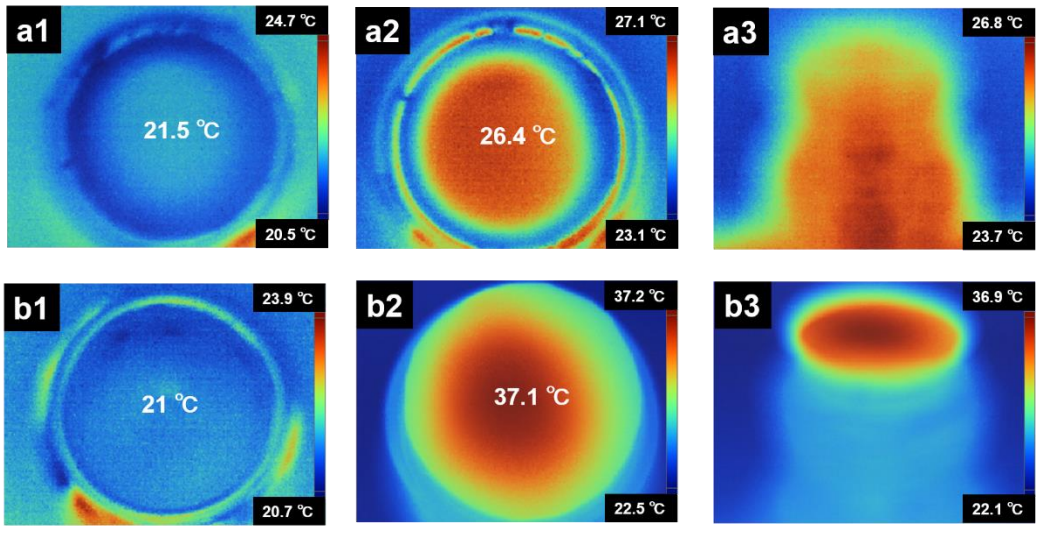

Fig. 4. IR images showing temperature distribution of the initial surface (a1, b1), surface after

30 mins irradiation (a2, b2), and cross-sectional view after 30 min irradiation (a3, b3) of (a) pure water and (b) pure water with EPE foam supported MDPC/SS mesh floating on the top.

In the following, the water evaporation performance of the prepared MDPC/SS mesh was investigated. Fig. 5a displays the schematic setup for evaluating the water evaporation performance. The bilayer device with high light absorption, low thermal conductivity, good hydrophilic property, and buoyant nature demonstrates the promising potential for solar steam generation with water constantly evaporating at the air-water interface, as represented in Fig. 5b. Moreover, the unique porous frameworks of MDPC with vertically aligned structures are favorable for the generated vapor to escape, which are beneficial for efficient solar steam generation. As a reference, the evaporation system using only water, water with floating air-laid paper wrapped EPE foam, and water with EPE foam supported bare SS mesh were measured as well. Fig. 6a shows the corresponding time-dependent mass changes under one sun (1kW m^{-2}) irradiation, which subtracted the corresponding spontaneous evaporation rate under the dark field included in the supplementary file (Fig. S4). As it is nicely seen in Fig. 6a, the water evaporation in the presence of MDPC/SS mesh is significantly enhanced compared to that of pure water. The evaporation performance of air-laid paper wrapped EPE foam is closed to that of pure water, indicating a very little effect of EPE foam on the solar steam generation. EPE foam only serves as a thermal insulator and supports to the MDPC/SS mesh.

Nevertheless, after 60 min of irradiation, the mass change of the system with MDPC/SS mesh reached to 1.222 kg m^{-2}, which is more than 5 times higher than that of pure water (0.208 kg m^{-2}). Besides, the solar steam generation performances of MDPC/SS meshes with different mass loading of MDPC were investigated, which were fabricated by immersing the SS mesh into the reaction mixture for 0.5 h and 2 h, respectively, and followed by the same carbonization process. The two obtained samples both present relatively worse evaporation performance than that of MDPC/SS mesh with growth time of 1 h (Fig. S5a) due to the higher light reflection (Fig. S5b). With the reaction time of 0.5 h, the surface of SS mesh was not fully covered by vertically aligned MDPC (Fig. S5c), while increasing the reaction time to 2 h, larger and irregularly aligned MDPC sheets appeared (Fig. S5d). The incomplete coverage and irregularly aligned large MDPC sheets can reduce the multi-scattering and light trapping effect in the samples, leading to a higher light reflection. Furthermore, the evaporation performance of a filtered MDPC film was also evaluated. The MDPC film was obtained by vacuum filtration of MCE membrane being a substrate instead of 3D SS mesh (Fig. S6a). As shown in Fig. S6b of the Supplementary file, the filtered MDPC film displays a lower mass change compared to the case with MDPC/SS mesh, resulting from a relatively higher reflection of the incident light than that of the MDPC/SS mesh as provided in the Supplementary Fig. S6c. The strategy of depositing the photo-thermal materials on a membrane via vacuum filtration has been frequently reported in several literatures [49, 50], in which the absorbers are fragile due to the

weak linkage between the photo-thermal materials and the membranes. Besides, the 3D structure can also improve the solar evaporation efficiency by providing efficient water transport channels for vapor generation and escape. Hence, it is appealing to deposit the photo-thermal materials onto the 3D substrate with mechanical strength. Moreover, in order to confirm that the substrate is not limited to SS mesh, the MDPC coated on Ni foam (MDPC/NF) and carbon cloth (MDPC/CC) were further prepared, and the corresponding water evaporation performance was evaluated, as shown in Fig. S7. The mass changes of the MDPC/NF and MDPC/CC were much improved than that of pure water and bare substrate as well, but slightly lower than that of MDPC/SS mesh. This is due to the fact that a portion of incident light can directly transmit through the Ni foam and carbon cloth, resulting in lower light absorption. These results demonstrate that deposition of MDPC on the lightproof 3D substrate is a feasible and promising method for efficient solar steam generation.

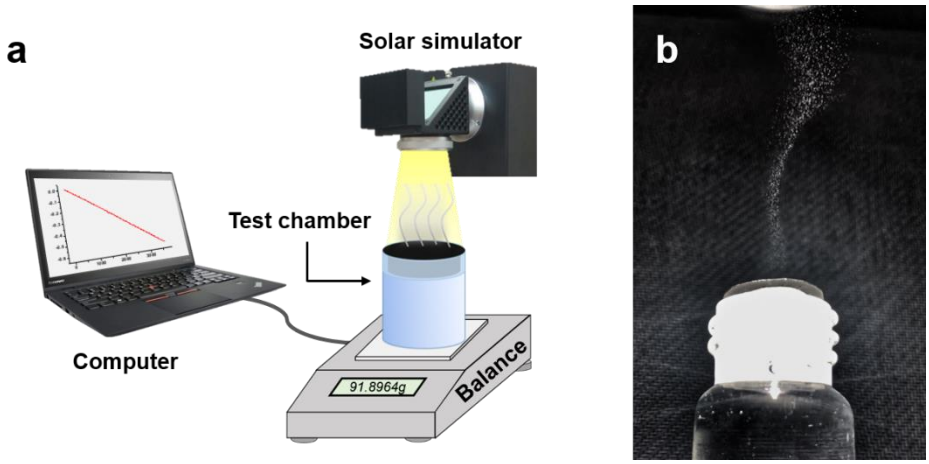

Fig. 5. (a) Schematic test system for the solar water evaporation experiment. (b) Digital image

of the generated steam enabled by the MDPC/SS mesh under 5 kW m^{-2}.

The photo-thermal conversion efficiency (η_{th}) of the samples was calculated by the following equation [51, 52]:

$$\eta_{\mathrm{th}} = \frac{\dot{m} h_{LV}}{I}$$

where $\dot{m}$ is the water evaporation rate under a steady state excluding the evaporation rate under the dark field, h_{LV} is the total enthalpy of the liquid-vapor phase change containing the sensible heat and the latent heat of evaporation, and I refers to the power density of the light irradiation on the absorber surface. Under one sun illumination, the photo-thermal efficiency of the MDPC/SS mesh reaches as high as 84.3% (Fig. 6b), which favorably stands against that of pure water, whose conversion efficiency is only 14.2% (see detailed calculation in the Supplementary Note and Table S1). The photo-thermal conversion efficiency of the current system is comparable with many of the previously reported solar evaporators (Table S2). The mass change of the MDPC/SS mesh under a higher light density of 5 kW m^{-2} was also measured. As shown in Fig. 6c, the evaporation rate reached 5.645 kg m^{-2} h^{-1} with a photo-thermal conversion efficiency of 78.8%. This efficiency is less than that of MDPC/ SS mesh under the lower light density of 1 kW m^{-2}, which is analyzed due to the increased heat loss under a higher irradiation density [42, 53]. The recyclability of the MDPC/SS mesh was further valued by repeating the experiment of solar steam generation for 15 cycles. For each cycle, the same

MDPC/SS mesh was used and illuminated for 1h under a light density of 1 kW m^{-2}. The results in Fig. 6d show that the mass change was relatively stable with the variation of < 3%, and the morphology of the MDPC/SS mesh was well kept with no MDPC peeled off (as shown in the Supplementary Fig. S8a and S8b). Moreover, after soaking in water for two weeks, the evaporation rate of the MDPC/SS mesh shows no obvious change as presented in the Supplementary Fig. S8c. The recyclability and stability tests indicate that the MDPC/SS mesh prepared by depositing the MDPC on the SS mesh has excellent mechanical strength and performance stability for the solar evaporation application.

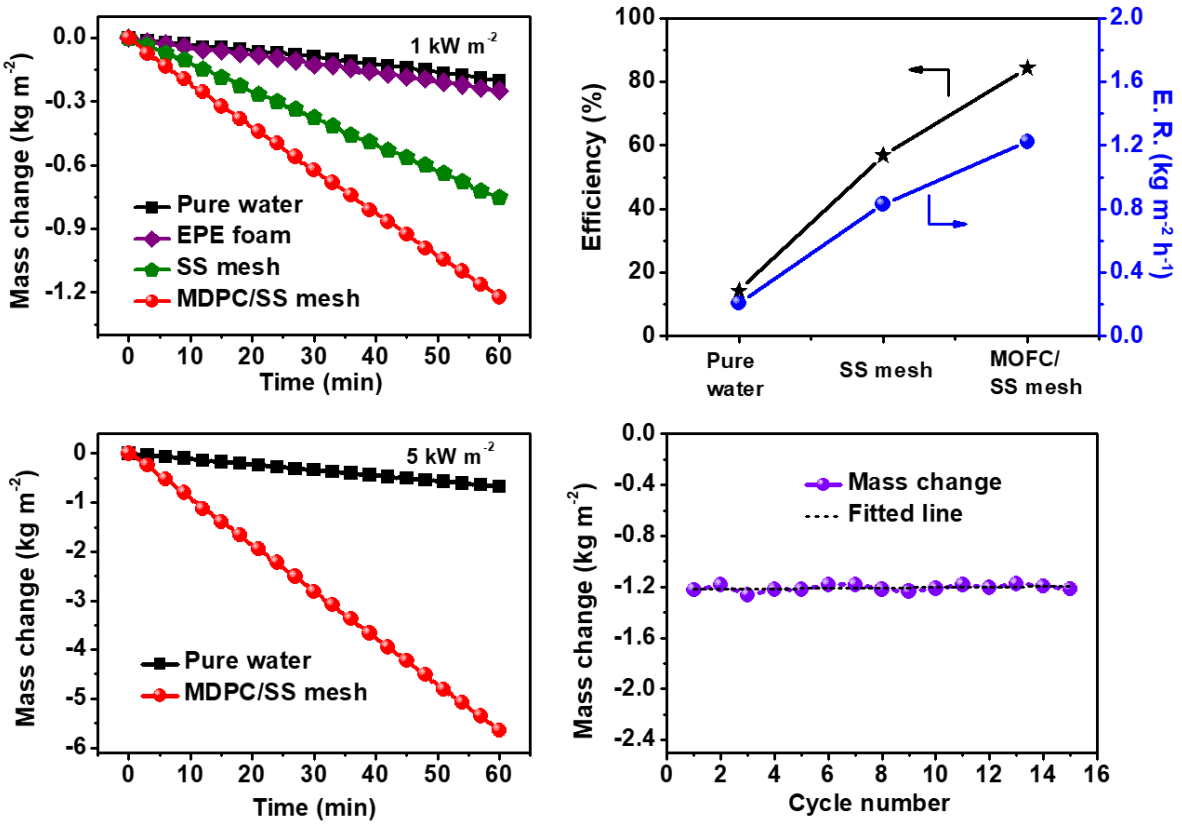

Fig. 6. (a) The evaporation mass change over time of the system with different evaporators under 1 kW m^{-2} illumination. (b) The water evaporation rate and photo-thermal conversion

efficiency of pure water, bare SS mesh, and MDPC/SS mesh. (c) The evaporation mass change over time with and without MDPC/SS mesh under a light density of 5 kW m^{-2}. (d) The cyclic performance of the MDPC/SS mesh for water evaporation for 1h over 15 cycles. The evaporations under the dark field were subtracted.

To evaluate the potential ability of the MDPC/SS mesh for seawater desalination, the desalination experiment was conducted on a homemade setup with simulated seawater, as shown in Fig. 7a and the Supplementary Fig. S9. The simulated seawater was prepared by mixing 6.68 g of NaCl, 0.05 g of $NaHCO_3$, 0.87 g of Na_2SO_4, 0.18 g of KCl, 0.57 g of $MgCl_2$, 0.81 g of $MgSO_4$, and 0.28 g of $CaCl_2$ in 250 mL of DI water [54]. After solar illumination, the desalinated water was condensed in the chamber and collected to measure the ions (Na^+, K^+, Mg^{2+}, Ca^{2+}) concentrations by inductive-coupled plasma mass spectrometry. As presented in Fig. 7b and Table S3 of the supplementary file, after desalination, the concentrations of the four ions are reduced by 4-5 orders of magnitude in contrast to the originally simulated seawater, which are far below the standards of safe drinking water for the salinity of 200 mg L^{-1}defined by the World Health Organization [53, 55]. Note that the SS mesh as a metal-based material still faces the common issue of erosion in seawater over a long time. The desalination performance of MDPC/CC using carbon cloth as substrate was investigated as well, which is comparable to that of MDPC/SS mesh (Table S3 in the Supplementary). Further works with

anti-corrosive substrates can be explored in future. It is convinced that the MDPC with light trapping structures acting as solar absorber can be a promising candidate in the solar desalination.

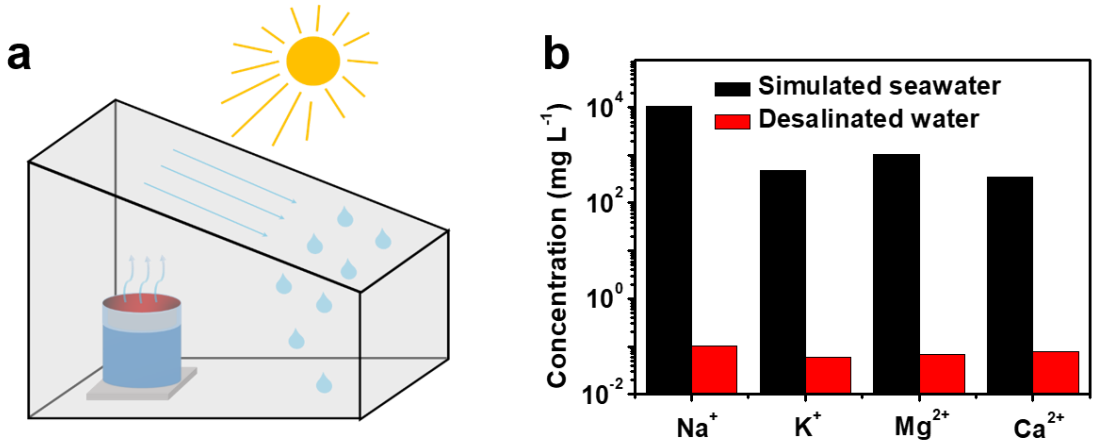

Fig. 7. (a) Schematic of the homemade setup for seawater desalination. (b) The concentrations of Na^+, K^+, Mg^{2+}, and Ca^{2+} irons before and after desalination.

4. Conclusion

For the first time, a highly efficient solar thermal evaporator consisting of MDPC/SS mesh supported by the floatable EPE foam was demonstrated for interfacial solar steam generation. The MDPC/SS mesh was synthesized by a facial solvent method by depositing the leaf-like MOF precursor on the SS mesh, followed by an annealing process. Our as-prepared evaporator not only exhibits a high photo-thermal conversion efficiency of 84.3% with an evaporation rate of 1.222 kg m^{-2} h^{-1} under one sun illumination but also achieves effective solar desalination.

The outstanding performance is attributed to the unique light trapping structures of the MDPC/SS mesh for high solar light absorption, excellent hydrophilicity that enables fluent water permeation, and heat localization for interfacial evaporation. Furthermore, the MDPC/SS mesh presents good recyclability and long-term stability while applied in the water evaporation. Meanwhile, the substrate in our system is not limited to the SS mesh, whereas other porous substrates like Ni foam and carbon cloth. Thus, the current findings reveal that the MOF derived carbon can be a promising photo-thermal material for future solar steam generation and related water regeneration systems. It will trigger further research with wide potential applications of MOF materials for the solar thermal absorber developments.

Acknowledgments

This work is financially supported by the Shenzhen Science and Technology Innovation Commission, the Fundamental Research Funds (JCYJ20170303160136888) and (JCYJ201605313001154), National Natural Science Foundation of China (61575167), and the Research Grants Council of Hong Kong, China (GRF 152109/16E PolyU B-Q52T).

Reference

[1] J. Bartram, C. Brocklehurst, M. Fisher, R. Luyendijk, R. Hossain, T. Wardlaw, B. Gordon, Global monitoring of water supply and sanitation: history, methods and future challenges, Int. J. Env. Res. Pub. He. 11(8) (2014) 8137.

[2] M. Elimelech, W.A. Phillip, The future of seawater desalination: energy, technology, and

the environment, Science 333(6043) (2011) 712-717.
[3] S.L. Postel, G.C. Daily, P.R. Ehrlich, Human appropriation of renewable fresh water, Science 271(5250) (1996) 785-788.
[4] S.W. Sharshir, G. Peng, N. Yang, M.O.A. El-Samadony, A.E. Kabeel, A continuous desalination system using humidification-dehumidification and a solar still with an evacuated solar water heater, Appl. Therm. Eng. 104 (2016) 734-742.
[5] H. Li, Y. He, Z. Liu, Y. Huang, B. Jiang, Synchronous steam generation and heat collection in a broadband Ag@TiO_2 core-shell nanoparticle-based receiver, Appl. Therm. Eng. 121 (2017) 617-627.
[6] Z. Deng, J. Zhou, L. Miao, C. Liu, Y. Peng, L. Sun, S. Tanemura, The emergence of solar thermal utilization: solar-driven steam generation, J. Mater. Chem. A 5(17) (2017) 7691-7709.
[7] A. Lenert, E.N. Wang, Optimization of nanofluid volumetric receivers for solar thermal energy conversion, Sol. Energy 86(1) (2012) 253-265.
[8] G. Ahmadi, D. Toghraie, A. Azimian, O.A. Akbari, Evaluation of synchronous execution of full repowering and solar assisting in a 200mW steam power plant, a case study, Appl. Therm. Eng. 112 (2017) 111-123.
[9] H. Ghasemi, G. Ni, A.M. Marconnet, J. Loomis, S. Yerci, N. Miljkovic, G. Chen, Solar steam generation by heat localization, Nat. Commun. 5 (2014) 4449.
[10] L. Zhang, B. Tang, J. Wu, R. Li, P. Wang, Hydrophobic light-to-heat conversion membranes with self-healing ability for interfacial solar heating, Adv. Mater. 27(33) (2015) 4889-4894.
[11] G. Ni, G. Li, Svetlana V. Boriskina, H. Li, W. Yang, T. Zhang, G. Chen, Steam generation under one sun enabled by a floating structure with thermal concentration, Nat. Energy 1 (2016) 16126.
[12] S. Ma, C.P. Chiu, Y. Zhu, C.Y. Tang, H. Long, W. Qarony, X. Zhao, X. Zhang, W.H. Lo, Y.H. Tsang, Recycled waste black polyurethane sponges for solar vapor generation and distillation, Appl. Energy 206 (2017) 63-69.
[13] J. Li, M. Du, G. Lv, L. Zhou, X. Li, L. Bertoluzzi, C. Liu, S. Zhu, J. Zhu, Interfacial solar steam generation enables fast-responsive, energy-efficient, and low-cost off-grid sterilization, Adv. Mater. 30(49) (2018) 1805159.
[14] X. Li, J. Li, J. Lu, N. Xu, C. Chen, X. Min, B. Zhu, H. Li, L. Zhou, S. Zhu, T. Zhang, J. Zhu, Enhancement of interfacial solar vapor generation by environmental energy, Joule 2(7) (2018) 1331-1338.
[15] L. Zhou, Y. Tan, D. Ji, B. Zhu, P. Zhang, J. Xu, Q. Gan, Z. Yu, J. Zhu, Self-assembly of highly efficient, broadband plasmonic absorbers for solar steam generation, Sci. Adv. 2(4) (2016).
[16] M. Zhu, Y. Li, F. Chen, X. Zhu, J. Dai, Y. Li, Z. Yang, X. Yan, J. Song, Y. Wang, E. Hitz, W. Luo, M. Lu, B. Yang, L. Hu, Plasmonic wood for high-efficiency solar steam generation,

Adv. Energy Mater. 8(4) (2017) 1701028.
[17] J. Yang, Y. Pang, W. Huang, S.K. Shaw, J. Schiffbauer, M.A. Pillers, X. Mu, S. Luo, T. Zhang, Y. Huang, G. Li, S. Ptasinska, M. Lieberman, T. Luo, Functionalized graphene enables highly efficient solar thermal steam generation, ACS Nano 11(6) (2017) 5510-5518.
[18] Y. Ito, Y. Tanabe, J. Han, T. Fujita, K. Tanigaki, M. Chen, Multifunctional porous graphene for high-efficiency steam generation by heat localization, Adv. Mater. 27(29) (2015) 4302-4307.
[19] C. Chen, L. Zhou, J. Yu, Y. Wang, S. Nie, S. Zhu, J. Zhu, Dual functional asymmetric plasmonic structures for solar water purification and pollution detection, Nano Energy 51 (2018) 451-456.
[20] Z. Wang, Y. Liu, P. Tao, Q. Shen, N. Yi, F. Zhang, Q. Liu, C. Song, D. Zhang, W. Shang, T. Deng, Bio-inspired evaporation through plasmonic film of nanoparticles at the air-water interface, Small 10(16) (2014) 3234-3239.
[21] L. Zhou, Y. Tan, J. Wang, W. Xu, Y. Yuan, W. Cai, S. Zhu, J. Zhu, 3D self-assembly of aluminium nanoparticles for plasmon-enhanced solar desalination, Nat. Photon. 10 (2016) 393.
[22] Q. Jiang, L. Tian, K.-K. Liu, S. Tadepalli, R. Raliya, P. Biswas, R.R. Naik, S. Singamaneni, Bilayered biofoam for highly efficient solar steam generation, Adv. Mater. 28(42) (2016) 9400-9407.
[23] X. Hu, W. Xu, L. Zhou, Y. Tan, Y. Wang, S. Zhu, J. Zhu, Tailoring graphene oxide-based aerogels for efficient solar steam generation under one sun, Adv. Mater. 29(5) (2016) 1604031.
[24] X. Zhou, F. Zhao, Y. Guo, Y. Zhang, G. Yu, A hydrogel-based antifouling solar evaporator for highly efficient water desalination, Energy Environ. Sci. 11(8) (2018) 1985-1992.
[25] Y. Wang, L. Zhang, P. Wang, Self-floating carbon nanotube membrane on macroporous silica substrate for highly efficient solar-driven interfacial water evaporation, ACS Sustain. Chem. Eng. 4(3) (2016) 1223-1230.
[26] W. Xu, X. Hu, S. Zhuang, Y. Wang, X. Li, L. Zhou, S. Zhu, J. Zhu, Flexible and salt resistant janus absorbers by electrospinning for stable and efficient solar desalination, Adv. Energy Mater. 8(14) (2018) 1702884.
[27] G. Xue, K. Liu, Q. Chen, P. Yang, J. Li, T. Ding, J. Duan, B. Qi, J. Zhou, Robust and low-cost flame-treated wood for high-performance solar steam generation, ACS Appl. Mater. Inter. 9(17) (2017) 15052-15057.
[28] N. Xu, X. Hu, W. Xu, X. Li, L. Zhou, S. Zhu, J. Zhu, Mushrooms as efficient solar steam-generation devices, Adv. Mater. 29(28) (2017) 1606762.
[29] L. Shi, Y. Wang, L. Zhang, P. Wang, Rational design of a bi-layered reduced graphene oxide film on polystyrene foam for solar-driven interfacial water evaporation, J. Mater. Chem. A 5(31) (2017) 16212-16219.
[30] H. Furukawa, K.E. Cordova, M. O'Keeffe, O.M. Yaghi, The chemistry and applications of metal-organic frameworks, Science 341(6149) (2013).

[31] H.-C. Zhou, J.R. Long, O.M. Yaghi, Introduction to metal-organic frameworks, Chem. Rev. 112(2) (2012) 673-674.
[32] S.J. Yang, T. Kim, J.H. Im, Y.S. Kim, K. Lee, H. Jung, C.R. Park, Mof-derived hierarchically porous carbon with exceptional porosity and hydrogen storage capacity, Chem. Mater. 24(3) (2012) 464-470.
[33] S. Jung, W. Cho, H.J. Lee, M. Oh, Self-template-directed formation of coordination-polymer hexagonal tubes and rings, and their calcination to ZnO rings, Angew. Chem. 121(8) (2008) 1487-1490.
[34] C. Guan, X. Liu, W. Ren, X. Li, C. Cheng, J. Wang, Rational design of metal-organic framework derived hollow $NiCo_2O_4$ arrays for flexible supercapacitor and electrocatalysis, Adv. Energy Mater. 7(12) (2017) 1602391.
[35] X.-F. Lu, L.-F. Gu, J.-W. Wang, J.-X. Wu, P.-Q. Liao, G.-R. Li, Bimetal-organic framework derived $CoFe_2O_4$/C porous hybrid nanorod arrays as high-performance electrocatalysts for oxygen evolution reaction, Adv. Mater. 29(3) (2016) 1604437.
[36] X. Li, Y. Fang, X. Lin, M. Tian, X. An, Y. Fu, R. Li, J. Jin, J. Ma, MoF derived Co_3O_4 nanoparticles embedded in N-doped mesoporous carbon layer/MWCNT hybrids: extraordinary bi-functional electrocatalysts for OER and ORR, J. Mater. Chem. A 3(33) (2015) 17392-17402.
[37] K. Shen, X. Chen, J. Chen, Y. Li, Development of MOF-derived carbon-based nanomaterials for efficient catalysis, ACS Catal. 6(9) (2016) 5887-5903.
[38] A. Banerjee, R. Gokhale, S. Bhatnagar, J. Jog, M. Bhardwaj, B. Lefez, B. Hannoyer, S. Ogale, MOF derived porous carbon-Fe_3O_4 nanocomposite as a high performance, recyclable environmental superadsorbent, J. Mater. Chem. 22(37) (2012) 19694-19699.
[39] X.-H. Zhao, S.-N. Ma, H. Long, H. Yuan, C.Y. Tang, P.K. Cheng, Y.H. Tsang, Multifunctional sensor based on porous carbon derived from metal-organic frameworks for real time health monitoring, ACS Appl. Mater. Inter. 10(4) (2018) 3986-3993.
[40] Z. Wei, W. Zhu, Y. Li, Y. Ma, J. Wang, N. Hu, Y. Suo, J. Wang, Conductive leaflike cobalt metal–organic framework nanoarray on carbon cloth as a flexible and versatile anode toward both electrocatalytic glucose and water oxidation, Inorg. Chem. 57(14) (2018) 8422-8428.
[41] C. Guan, W. Zhao, Y. Hu, Z. Lai, X. Li, S. Sun, H. Zhang, A.K. Cheetham, J. Wang, Cobalt oxide and N-doped carbon nanosheets derived from a single two-dimensional metal–organic framework precursor and their application in flexible asymmetric supercapacitors, Nanoscale Horiz. 2(2) (2017) 99-105.
[42] D. Hao, Y. Yang, B. Xu, Z. Cai, Efficient solar water vapor generation enabled by water-absorbing polypyrrole coated cotton fabric with enhanced heat localization, Appl. Therm. Eng. 141 (2018) 406-412.
[43] D. Li, H. Liao, H. Kikuchi, T. Liu, Microporous Co@C nanoparticles prepared by dealloying CoAl@C precursors: achieving strong wideband microwave absorption via controlling carbon shell thickness, ACS Appl. Mater. Inter. 9(51) (2017) 44704-44714.

[44] J. Mao, M. Ge, J. Huang, Y. Lai, C. Lin, K. Zhang, K. Meng, Y. Tang, Constructing multifunctional MOF@RGO hydro-/aerogels by the self-assembly process for customized water remediation, J. Mater. Chem. A 5(23) (2017) 11873-11881.
[45] Y. Li, T. Gao, Z. Yang, C. Chen, W. Luo, J. Song, E. Hitz, C. Jia, Y. Zhou, B. Liu, B. Yang, L. Hu, 3D-printed, all-in-one evaporator for high-efficiency solar steam generation under 1 sun illumination, Adv. Mater. 29(26) (2017) 1700981.
[46] Y. Bian, Q. Du, K. Tang, Y. Shen, L. Hao, D. Zhou, X. Wang, Z. Xu, H. Zhang, L. Zhao, S. Zhu, J. Ye, H. Lu, Y. Yang, R. Zhang, Y. Zheng, S. Gu, Carbonized bamboos as excellent 3D solar vapor-generation devices, Adv. Mater. Technol. (2018) 1800593.
[47] T. Gao, Y. Li, C. Chen, Z. Yang, Y. Kuang, C. Jia, J. Song, E.M. Hitz, B. Liu, H. Huang, J. Yu, B. Yang, L. Hu, Architecting a floatable, durable, and scalable steam generator: hydrophobic/hydrophilic bifunctional structure for solar evaporation enhancement, Small Methods (2018) 1800176.
[48] T.A. Cooper, S.H. Zandavi, G.W. Ni, Y. Tsurimaki, Y. Huang, S.V. Boriskina, G. Chen, Contactless steam generation and superheating under one sun illumination, Nat. Commun. 9(1) (2018) 5086.
[49] G. Wang, Y. Fu, X. Ma, W. Pi, D. Liu, X. Wang, Reusable reduced graphene oxide based double-layer system modified by polyethylenimine for solar steam generation, Carbon 114 (2017) 117-124.
[50] X. Li, W. Xu, M. Tang, L. Zhou, B. Zhu, S. Zhu, J. Zhu, Graphene oxide-based efficient and scalable solar desalination under one sun with a confined 2D water path, Proc. Natl. Acad. Sci. U. S. A. 113(49) (2016) 13953-13958.
[51] H. Li, Y. He, Y. Hu, X. Wang, Commercially available activated carbon fiber felt enables efficient solar steam generation, ACS Appl. Mater. Inter. 10(11) (2018) 9362-9368.
[52] X. Yin, Y. Zhang, Q. Guo, X. Cai, J. Xiao, Z. Ding, J. Yang, Macroporous double-network hydrogel for high-efficiency solar steam generation under 1 sun illumination, ACS Appl. Mater. Inter. 10(13) (2018) 10998-11007.
[53] M. Chen, Y. Wu, W. Song, Y. Mo, X. Lin, Q. He, B. Guo, Plasmonic nanoparticle-embedded poly(p-phenylene benzobisoxazole) nanofibrous composite films for solar steam generation, Nanoscale 10(13) (2018) 6186-6193.
[54] Y.-Y. Ma, C.-X. Wu, X.-J. Feng, H.-Q. Tan, L.-K. Yan, Y. Liu, Z.-H. Kang, E.-B. Wang, Y.-G. Li, Highly efficient hydrogen evolution from seawater by a low-cost and stable CoMoP@C electrocatalyst superior to Pt/C, Energy Environ. Sci. 10(3) (2017) 788-798.
[55] WHO. Guidelines for drinking-water quality, recommendations, 3rd ed; World Health Organization: Geneva, 2006; Vol. 1.